Journal of Magnetic Resonance 313 (2020) 106702

Contents lists available at ScienceDirect

Journal of Magnetic Resonance

journal homepage: www.elsevier.com/locate/jmr

# Characterization of frequency-chirped dynamic nuclear polarization in rotating solids

Patrick T. Judge [b,c,1], Erika L. Sesti [b,1], Nicholas Alaniva [b], Edward P. Saliba [b], Lauren E. Price [b], Chukun Gao [b], Thomas Halbritter [d], Snorri Th. Sigurdsson [d], George B. Kyei [e,f], Alexander B. Barnes [a,b,*]

[a] Physical Chemistry, ETH Zurich, Vladimir-Prelog-Weg 2, 8093 Zurich, Switzerland
[b] Department of Chemistry, Washington University in St. Louis, St. Louis, MO 63130, United States
[c] Department of Biochemistry, Biophysics & Structural Biology, Washington University in St. Louis, St. Louis, MO 63110, United States
[d] Department of Chemistry, University of Iceland, Science Institute, Dunhaga 3, 107 Reykjavik, Iceland
[e] Department of Medicine, Washington University School of Medicine, St. Louis, MO 63130, United States
[f] Noguchi Memorial Institute for Medical Research, College of Health Sciences, University of Ghana, Legon, Accra, Ghana

ARTICLE INFO

*Article history:*
Received 29 October 2019
Revised 18 January 2020
Accepted 21 February 2020
Available online 29 February 2020

*Keywords:*
Dynamic nuclear polarization (DNP)
Frequency-chirped DNP
Pulsed DNP
Magic angle spinning NMR
Gyrotron

ABSTRACT

Continuous wave (CW) dynamic nuclear polarization (DNP) is used with magic angle spinning (MAS) to enhance the typically poor sensitivity of nuclear magnetic resonance (NMR) by orders of magnitude. In a recent publication we show that further enhancement is obtained by using a frequency-agile gyrotron to chirp incident microwave frequency through the electron resonance frequency during DNP transfer. Here we characterize the effect of chirped MAS DNP by investigating the sweep time, sweep width, center-frequency, and electron Rabi frequency of the chirps. We show the advantages of chirped DNP with a trityl-nitroxide biradical, and a lack of improvement with chirped DNP using AMUPol, a nitroxide biradical. Frequency-chirped DNP on a model system of urea in a cryoprotecting matrix yields an enhancement of 142, 21% greater than that obtained with CW DNP. We then go beyond this model system and apply chirped DNP to intact human cells. In human Jurkat cells, frequency-chirped DNP improves enhancement by 24% over CW DNP. The characterization of the chirped DNP effect reveals instrument limitations on sweep time and sweep width, promising even greater increases in sensitivity with further technology development. These improvements in gyrotron technology, frequency-agile methods, and in-cell applications are expected to play a significant role in the advancement of MAS DNP.



## 1. Introduction

Dynamic nuclear polarization (DNP) is commonly used to improve the inherent insensitivity of nuclear magnetic resonance (NMR) spectroscopy [1–13]. Typically, only continuous wave (CW) microwave methods have been employed with magic angle spinning (MAS) DNP. The solid effect and the cross effect are the primary DNP mechanisms used in moderate magnetic field strengths of 5–14 Tesla (T) [14–18]. While CW approaches can significantly increase NMR sensitivity, they have limitations. Except in certain model systems [6,19,20], the solid effect and cross effect are inefficient at room temperature due to short longitudinal electron relaxation times. To perform CW DNP, samples are commonly cooled to <120 K, which adds complexity not only to the instrumentation, but also often leads to a loss of spectral resolution [14,21]. Arrested molecular motion at these temperatures can cause substantial line broadening in most samples [3,21–23]. The cross effect and solid effect also exhibit worse performance at higher magnetic field, with cross effect efficiency decreasing as $1/B_0$ and that of solid effect as $1/B_0^2$ [15,24,25]. Therefore new mechanisms will be required for efficient DNP at magnetic fields of 28 T and higher.

Frequency-chirped DNP techniques, such as the frequency-swept integrated solid effect (FS-ISE) [15,26], nuclear orientation via electron spin locking (NOVEL) [27,28], and time-optimized pulsed (TOP) DNP [29] show promise to perform well both at high magnetic field and room temperature. For instance, ISE yields DNP enhancements of ~150 at room temperature and is predicted to be unaffected by the strength of the external magnetic field [15].

However, these experiments have been performed without MAS and at magnetic fields <3 T [15,27,29], primarily due to the diffi-

* Corresponding author at: Physical Chemistry, ETH Zurich, Vladimir-Prelog-Weg 2, 8093 Zurich, Switzerland.
*E-mail address:* abarnes@ethz.ch (A.B. Barnes).
[1] These authors contributed equally.

https://doi.org/10.1016/j.jmr.2020.106702
1090-7807/

culty of implementing MAS with the microwave resonators required to generate considerable electron nutation frequencies. Frequency-swept DNP at higher magnetic fields has also been shown to improve DNP performance [30,31], but has only recently been implemented with MAS [32,33]. MAS improves the sensitivity and resolution of solid-state NMR [34–38] by partially averaging anisotropic interactions of the magnetic resonance Hamiltonian, and is a crucial aspect of applying DNP to systems of interest.

Here we characterize the behavior of frequency-chirped DNP experiments performed with MAS, expanding on our recent work [32]. We optimize frequency chirps from a custom-built frequency-agile high-power gyrotron [39] to produce large gains in intensity beyond those obtained with CW DNP. In addition to measuring its performance on a model system, we conduct optimized chirped experiments on intact human Jurkat cells to demonstrate frequency-chirped DNP in a biologically complex environment.

## 2. Materials and methods

### 2.1. NMR experiments

MAS DNP NMR experiments were performed using a custom-built DNP spectrometer at a magnetic field of 7.1584 T [41]. $^{13}C$ and $^{1}H$ Larmor frequencies were 75.4937 MHz and 300.1790 MHz, respectively. A CPMAS, rotor synchronized, Hahn echo sequence with TPPM decoupling [42] was used for all experiments (Fig. 1a). The initial magnetization of $^{1}H$ and $^{13}C$ spins was destroyed using a saturation train. $^{1}H$ and $^{13}C$ pulses were performed with nutation frequencies of 77 kHz and 100 kHz, respectively. The Hartmann-Hahn matching condition ($\gamma B_1$) for $^{1}H$ and $^{13}C$ was 30 kHz. Frequency chirps were applied over the DNP polarization period ($\tau_{pol}$), and CW microwaves were employed over the rest of the experiment. The spinning frequency was 4.5 kHz for all experiments, and the sample temperature was 90 K. Typical polarization times ($\tau_{pol}$) for optimized spectra were 5-times the $T_1$ of the sample in the absence of microwaves, in order to remove contamination of the data by differences in the nuclear $T_1$ and the $T_{1DNP}$.

Microwaves were generated using a frequency-agile gyrotron, whose output frequency was adjusted by varying the electron acceleration potential at the electron gun anode. An arbitrary waveform generator (AWG) integrated into the NMR spectrometer (Redstone, Tecmag Inc. Houston, TX) was used to generate a waveform, which ramped the output frequency of the gyrotron in a linear fashion through 197.670 GHz, the frequency of maximum DNP enhancement of the TEMTriPol-1 radical [39]. The frequency chirps were a triangular waveform, which was repeated over the entire polarization period. For frequency chirp optimization the incident microwave power, the center DNP microwave frequency, and the sweep width and sweep time of the individual chirps were varied. The center frequency of the sweeps was varied by changing the voltage at the gyrotron anode with the AWG amplified by a high-voltage amplifier (TREK, Inc. Lockport, NY). The sweep width corresponded to the frequency range of one sweep/chirp (either up or down) in MHz, and sweep time was the time to complete a sweep/chirp. Microwave power was attenuated from full power by inserting copper foil with slits cut in it into a gap in the waveguide to partially pass the microwave beam. The optimal power of 7 W incident on the sample was used for most experiments, which provided an estimated electron Rabi frequency of 0.43 MHz [43].

The $^{13}C$ carbonyl resonance was fit using DMfit [44] to determine resulting enhancement increases. For all optimization spectra, the magnitude of the Hahn echo was used to calculate the percent increase in intensity. All experiments were repeated four times to acquire adequate error values for the measurements.

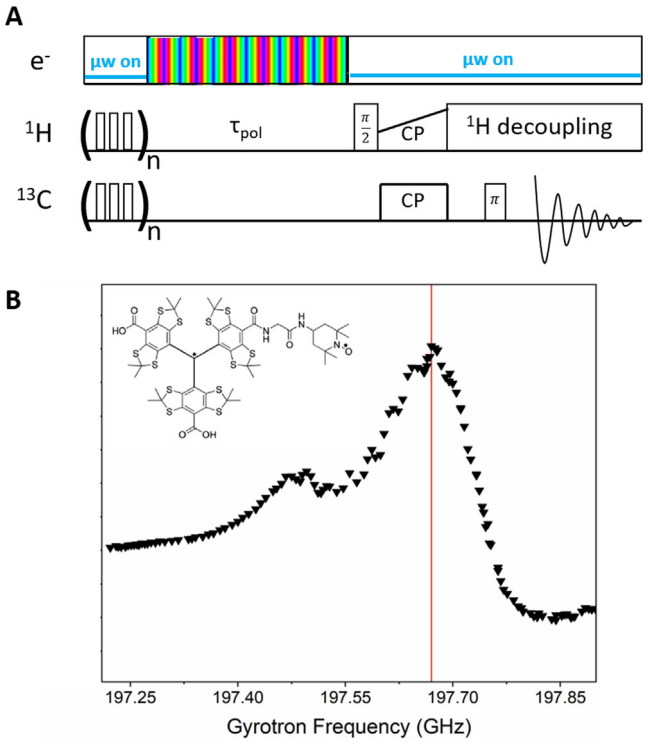


**Fig. 1.** Frequency-chirped DNP pulse sequence and $^{1}H$ enhancement profile of TEMTriPol-1. (a) The frequency-chirped DNP NMR pulse sequence. Triangular waveform frequency chirps (shown by the rainbow gradient) were applied over the polarization period ($\tau_{pol}$), while CW irradiation was applied during the remainder of the experiment. (b) Enhancement profile of TEMTriPol-1 using CW DNP. CPMAS experiments were performed with a $\tau_{pol}$ of 3 s at varying microwave frequencies to record a $^{1}H$ enhancement profile of the TEMTriPol-1 radical (shown in upper left corner). The red line represents the peak of Trityl's EPR resonance (197.670 GHz) as well as the center of the frequency chirps. This enhancement profile was adapted from Judge et al. [40] (For interpretation of the references to colour in this figure legend, the reader is referred to the web version of this article.)

### 2.2. Sample preparation

Experiments were performed on 4 M [U-$^{13}C$, $^{15}N$] urea mixed with 5 mM TEMTriPol-1 or 5 mM AMUPol in a cryoprotecting matrix consisting of 60% d8 glycerol, 30% $D_2O$, and 10% $H_2O$ by volume. Intact Jurkat cells (ATCC, Manassas, VA) were cultured in [U-$^{13}C$, 98%; U-$^{15}N$, 98%] BioExpress-6000 mammalian cell growth medium (Cambridge Isotope Laboratories, Tewksbury, MA) at a concentration of $3 \times 10^6$ cells/mL in a six-well plate at 37 °C and 5% $CO_2$ for 48 h. $3.6 \times 10^7$ cells were collected, spun at 170 g for 5 min, washed with 1× phosphate-buffered saline (PBS), and spun again at 170 g for 5 min to remove extracellular NMR labels ($g = 9.8\ m/s^2$). 40 µL of 20 mM TEMTriPol-1 in 1× PBS with 10% DMSO was added to a cell pellet containing 36 million Jurkat cells. This suspension was centrifuged directly into the 3.2 mm zirconia rotor at 800 g for 30 s and immediately frozen in liquid nitrogen as detailed in our previous work [4].

## 3. Results and discussion

Frequency-chirped DNP refers to a change in the microwave frequency or intensity throughout the course of an experiment. The frequency-chirped DNP pulse sequence is shown in Fig. 1A. Frequency chirps (represented by the rainbow gradient) are applied over the DNP polarization period and the resulting NMR signal is detected through a cross polarization (CP) Hahn echo sequence. We emphasize that microwave frequency chirps result

in better manipulation of the electron spin polarization, yet the active DNP mechanism is still the cross effect.

Selection of appropriate radicals for frequency-chirped DNP is crucial due to drastic differences in electron spin g-anisotropy and relaxation properties. In our previous demonstrations of electron decoupling using chirped microwave pulses with MAS, we employed trityl rather than nitroxide radicals [3,22]. Those successes led us to explore the use of trityl-nitroxide biradicals, with the rationale that the narrow trityl resonance would be easier to manipulate and the tethered nitroxide would provide greater DNP enhancements through the cross effect mechanism. TEMTriPol-1 is such a biradical, consisting of a Finland trityl radical covalently linked to a 4-amino TEMPO radical, which is used for cross effect DNP [13,45]. TEMTriPol-1 improves cross effect efficiency at high magnetic fields. Where other biradicals, such as AMUPol, depolarize nuclear spins at 100 K in the absence of microwave irradiation, TEMTriPol-1 preserves nuclear polarization [5,46].

### 3.1. Frequency-chirped DNP on a model system

CW DNP CPMAS experiments were performed at various microwave frequencies to record a $^{1}$H DNP enhancement profile with TEMTriPol-1 [40]. The enhancement profile shows the trityl resonance frequency as the optimal frequency for CW DNP enhancement. This will be the target for the center of the frequency chirps. In a 7.1584 T magnetic field, the microwave frequency for maximum CW DNP enhancement was 197.670 GHz (Fig. 1B).

Experiments were performed to determine the effect of frequency-chirped microwave pulses during the polarization period of MAS DNP (Fig. 2). For comparison, cross effect DNP experiments were performed with CW microwave irradiation. CW DNP experiments on a model system of urea with TEMTriPol-1 resulted in an enhancement of 118 (Fig. 2, red). Enhancements herein are defined as the NMR signal intensity recorded with DNP compared to that without DNP [46]. For frequency-chirped DNP experiments, the microwave frequency was linearly chirped with a triangular waveform over 197.670 GHz, with a 28 μs sweep time and a 120 MHz sweep width. These optimized chirps yielded a 21% increase over CW DNP and an enhancement of 142 (Fig. 2, blue). Polarization times of 53 s (5 × $T_{1DNP}$, Fig. S1) were used to ensure that >99% of the polarization had built up for both experiments, allowing for direct comparison of the CW and frequency-chirped experiments.

To determine the necessity of a narrow-line radical, such as trityl, for frequency-chirped DNP, experiments were performed on a sample containing the nitroxide-nitroxide biradical, AMUPol. The frequency chirps were centered at 197.674 GHz (maximum with $^{1}$H-enhancement for AMUPol) the previously optimized sweep time of 28 μs and sweep width of 120 MHz were used. Frequency chirps over the polarization period resulted in a decrease in signal intensity of 3% compared to CW DNP (Fig. 3). These frequency chirps do not yield the same improved electron spin control over the nitroxide biradical, AMUPol, as they do over TEMTriPol-1. This implies that a narrow-line radical is required for implementation of frequency-chirped DNP.

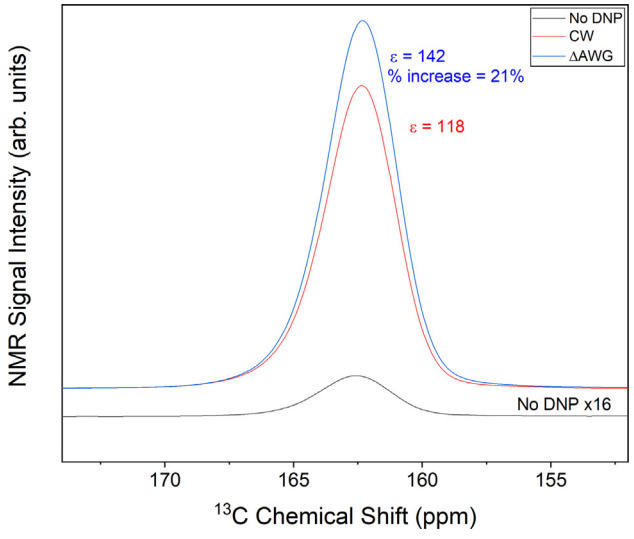


**Fig. 2.** Frequency-chirped DNP with TEMTriPol-1. Comparison of DNP spectra with triangular frequency sweeps (blue) and CW (red) microwave irradiation using 7 W of microwave power incident on the sample. The spectrum with no microwave irradiation is shown in black. The triangular frequency chirps generated an increase of 21% over CW DNP. The DNP polarization period for all three experiments was 53 s, the sweep width was 120 MHz, and the sweep time was 28 μs. (For interpretation of the references to colour in this figure legend, the reader is referred to the web version of this article.)

### 3.2. Frequency-chirped DNP in intact Jurkat cells

The performance of frequency-chirped DNP was then examined within intact human Jurkat cells (Fig. 4). Frequency chirps improved the NMR signal by 24%, yielding an enhancement of 6 (versus 4.8 for CW DNP). These results display the application of frequency-chirped DNP to more complex samples of biological interest.

### 3.3. Power dependence of CW and frequency-chirped DNP

To determine the dependence of CW and frequency-chirped enhancement on microwave power, CPMAS experiments were performed with varying microwave attenuation on the TEMTriPol-1/urea sample (Fig. 5). For frequency-chirped DNP the optimized triangle waveform (28 μs sweep time and 120 MHz sweep width) was repeated over a polarization time of 20 s. 35 W of microwave power incident on the sample (Rabi frequency of 0.95 MHz) produced a 123% increase in signal with frequency-chirped DNP compared to CW, yielding enhancements of 17 and 8, respectively

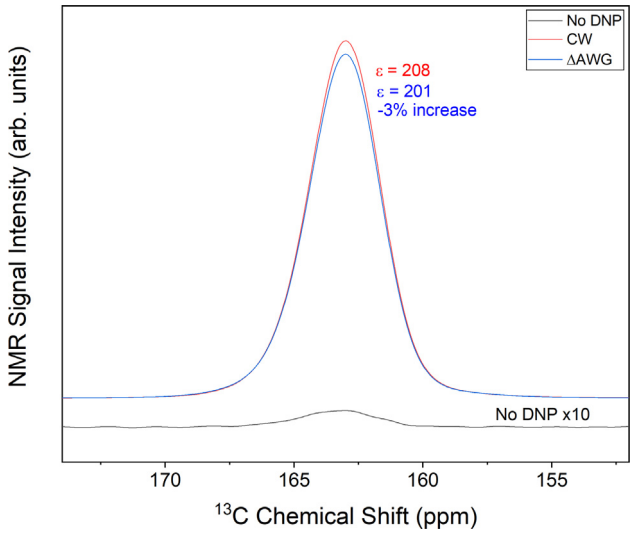


**Fig. 3.** Frequency-chirped DNP with AMUPol. The polarization time was 47 s with a sweep time of 28 μs and sweep width of 120 MHz centered at 197.674 GHz. Frequency chirps (blue) decreased the signal intensity by 3% compared to CW (red), providing an enhancement of 201 compared to an experiment with no microwaves incident on the sample (black). (For interpretation of the references to colour in this figure legend, the reader is referred to the web version of this article.)

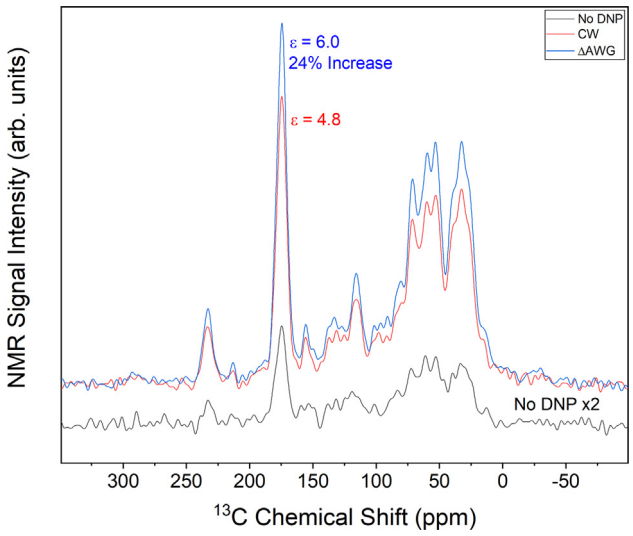


**Fig. 4.** Frequency-chirped MAS DNP in intact human cells. The polarization time was 10 s (5 × $T_{1DNP}$, Fig. S1). Frequency chirps (blue) resulted in a 24% improvement in overall signal intensity compared to CW (red) and enhanced the NMR signal by 6 times compared to signal without DNP (black). (For interpretation of the references to colour in this figure legend, the reader is referred to the web version of this article.)

(Fig. 5a, b). We note that such high microwave powers place the cross effect in the oversaturated regime, leading to less overall enhancement.

7 W of microwave power resulted in the highest sensitivity and an improvement of 25% with frequency-chirped DNP compared to CW. Higher microwave power yielded greater improvements with frequency-chirped DNP over CW DNP, but the overall signal intensity obtained was suboptimal due to saturation of the cross effect [47].

### 3.4. Characterization of Frequency-chirped DNP

The effects of sweep time, sweep width, and center frequency on the improvement with frequency-chirped DNP over CW irradiation are shown in Fig. 6. For the sweep time dependence the polarization time was 20 s; the sweep width was held constant at 80 MHz, the incident microwave power at 7 W, and the center frequency at 197.670 GHz. Shorter sweep times increased the sensitivity to a greater extent than longer sweep times, with the greatest improvement over CW (15%) occurring with a 20 μs sweep time (Fig. 6a). Sweep times below 20 μs were not achievable with the current microwave frequency agility circuit, as the frequency output waveform became distorted. A sweep time of 150 μs resulted in only a 1% improvement in signal intensity over CW. We suspect that at longer sweep times electron spin saturation is lost through relaxation mechanisms.

The dependence of frequency-chirped DNP sensitivity on the sweep width of the frequency chirps is shown in Fig. 6b. For this dependence the polarization time was 20 s; the sweep time was held constant at 28 μs, the incident microwave power at 7 W, and the center frequency at 197.670 GHz. The improvement from the frequency chirps increased as the sweep width increased. A 120 MHz sweep width resulted in an improvement of 21%, while the signal intensity decreased by 1% with a sweep width of 10 MHz. Due to instrument limitations, sweep widths greater than 120 MHz could not be attained. This width is roughly that of the base of the trityl lineshape in the enhancement profile (Fig. 1b). We previously reported a similar optimal sweep width in electron decoupling experiments involving the Finland trityl radical [3]. Larger sweep widths provide microwave irradiation that is resonant with a greater number of trityl electron spins, enabling better electron spin control and improving the efficiency of frequency-chirped DNP.

During characterization it is important to consider multiple points on the enhancement profile. Fig. 6d provides a clear picture of the effect of frequency chirping, whereas Fig. 6c shows the potential for misinformation. The choice of irradiation frequency can lead to suspiciously high improvements due to difference in positive and negative enhancement regions between CW and frequency-chirped DNP. The CW enhancement profile shows maximum positive and negative enhancements at 197.670 GHz and 197.850 GHz, respectively (Fig. 6d). Frequency chirping at microwave frequencies lower than 197.750 GHz (positive enhancement), yielded greater enhancements than CW (Fig. 6d). However, at frequencies greater than 197.750 GHz (negative enhancement), the frequency-chirped DNP provided lower signal intensity than CW DNP.

Note that at this point we have simply demonstrated the methodology of performing frequency-chirped DNP experiments with TEMTriPol-1. To compare the sensitivity of the experiments with TEMTriPol-1 and AMUPol, we can divide the signal-to-noise

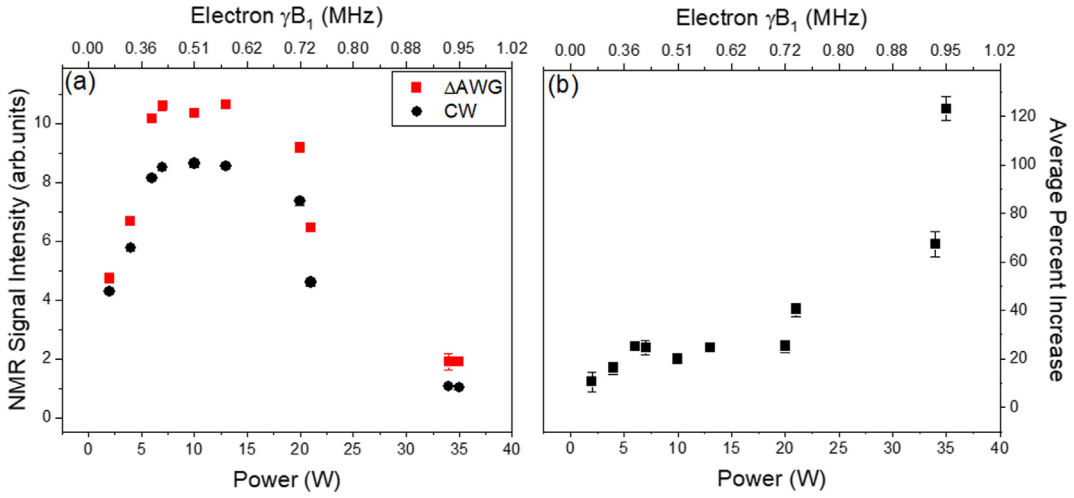


**Fig. 5.** Frequency-chirped DNP microwave power dependence. (a) Dependence of signal enhancement on incident microwave power, with and without frequency chirps. (b) Effect of microwave power on average percent increase in signal area with frequency chirps over CW.

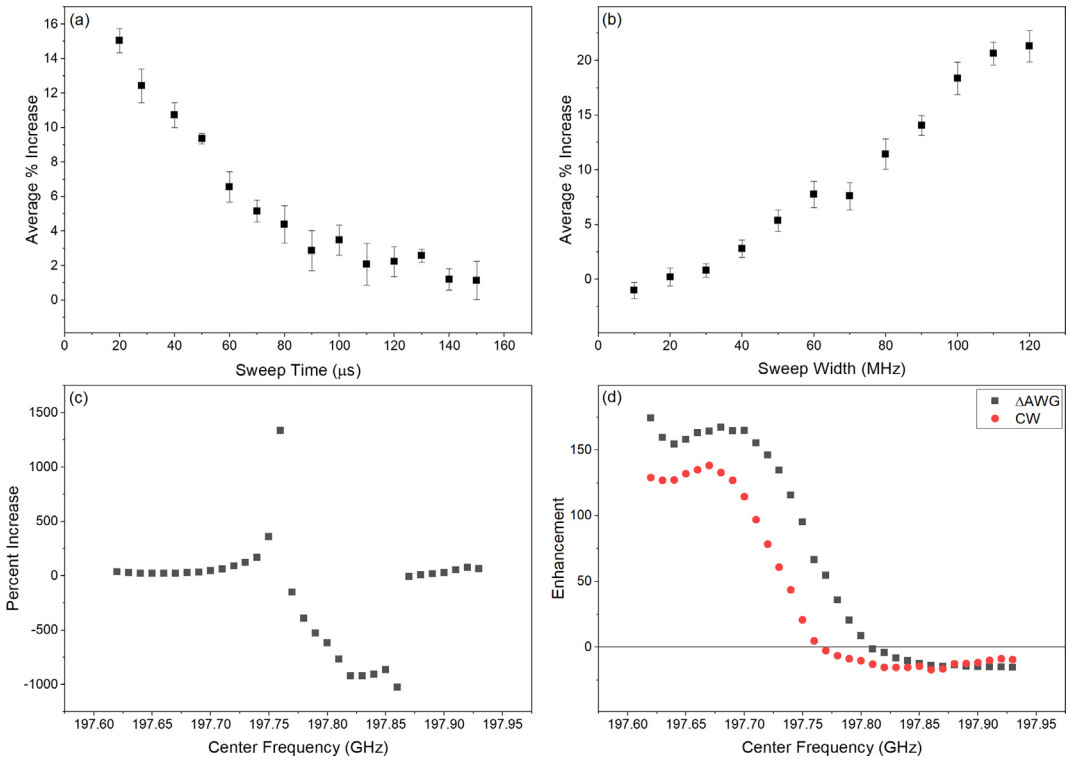


**Fig. 6.** Experimental parameter optimization for frequency-chirped DNP on urea with TEMTriPol-1. (a) Sweep time dependence using a 80 MHz sweep width centered at a gyrotron frequency of 197.670 GHz. (b) Sweep width dependence using a 28 μs sweep time centered at 197.670 GHz. (c) The percent increase of frequency-chirped DNP over CW DNP, using the points from the enhancement profile in (d). The order-of-magnitude larger increases/decreases are due to the different positive/negative enhancement crossing points for the two methods. (d) Enhancement profiles for CW DNP (red) and frequency-chirped DNP (black). A 20 s polarization time was used for all experiments. (For interpretation of the references to colour in this figure legend, the reader is referred to the web version of this article.)

from each experiment by the square root of the polarization time for the respective experiments. In doing so, we obtain a sensitivity of 79 with AMUPol (Fig. 3) and 73 with TEMTriPol-1 (Fig. 2). Thus, while the sensitivity of the experiments performed on each radical are similar at this stage, advances in instrumentation that enable greater sweep times and sweep widths will make frequency-chirped DNP experiments with TEMTriPol-1 more sensitive than AMUPol, and thus more feasible for sensitivity-demanding, multi-dimensional experiments.

## 4. Conclusion

To date, frequency-chirped DNP experiments, such as FS-ISE, NOVEL, and TOP DNP, have been largely restricted to static samples due to the difficulties of housing microwave resonators with the instrumentation required for magic angle spinning (MAS). Here, we have characterized the optimal experimental conditions for frequency-chirped MAS DNP. At a magnetic field of 7 T and with 7 W of microwave power, frequency-chirped microwaves over the polarization period improved DNP enhancements by 21%. Greater microwave powers resulted in up to 123% improvements with frequency-chirped DNP, but saturation of the cross effect resulted in less overall signal intensity.

These optimized frequency-chirped experiments were applied to a more biologically complex sample: intact Jurkat cells. This resulted in an improvement in signal intensity of 24% over CW DNP. Characterization of the parameters of frequency-chirped DNP revealed areas for further improvements to elicit even greater sensitivity. More powerful gyrotrons with larger frequency bandwidths, and gating mechanisms for chirps can be developed to increase sweep widths and shorten the sweep times, thus improving electron spin control. To take full advantage of frequency-chirped DNP at high power and high electron Rabi frequencies, duty cycling of the microwaves can be implemented to reduce dielectric heating [29]. We expect optimization of the waveform, with respect to both intensity and phase, to result in improved frequency-chirped DNP MAS performance. Future studies could analyze the effect of the spinning frequency on the enhancement achieved by frequency chirped DNP over CW DNP. Both the solid effect and cross effect are driven by interactions between the spin system, the microwave field, and the spinning rotor. Understanding these effects will prove crucial in the future development of DNP, as MAS frequencies and magnetic fields are pushed to ever higher values.

New radicals composed of tethered broad and narrow line radicals are currently being investigated with useful electronic properties such as long longitudinal relaxation times. Longer relaxation times will afford even more electron spin control with frequency-chirped DNP. Although the precise mechanism governing the improvement in sensitivity will require further investigation, it is possible that it is governed by an adiabatic process. As such, future experiments could focus on maintaining a constant sweep rate by simultaneously varying the sweep time and sweep width in an inverse manner. This could prove important, as adiabatic processes often show a remarkable resilience to microwave inhomogeneities and frequency offsets arising from difference in molecular orientation and conformations in a solid sample. These techniques can be paired with other advances in instrumentation such as higher power microwave sources and microwave lenses for improved microwave intensity and high frequency MAS for $^{1}$H detected spectra in future experiments. These could allow for the implementation of pulsed DNP mechanisms such as electron-nuclear cross polarization at high magnetic fields in the foreseeable future.

## Declaration of Competing Interest

The authors declare the following competing financial interest (s): A.B.B. is the author of a patent related to this work filed by the Washington University in Saint Louis (WO2015175507A1).

## Acknowledgment

The research reported in this publication was supported by an NIH Director's New Innovator Award [grant number DP2GM119131], an NSF CAREER Award [grant number DBI-1553577], a Camille Dreyfus Teacher-Scholar Award, a Deutsche Forschungsgemeinschaft (DFG) Postdoctoral Fellowship [414196920], and the University of Iceland Research Fund. We also thank Faith Scott, Sarah Overall, Asif Equbal, and Songi Han for helpful discussions.

## Appendix A. Supplementary material

Supplementary data to this article can be found online at https://doi.org/10.1016/j.jmr.2020.106702.

## References

[1] A.W. Overhauser, Polarization of nuclei in metals, Phys. Rev. 92 (1953) 411–415.
[2] T.R. Carver, C.P. Slichter, Polarization of nuclear spins in metals, Phys. Rev. 92 (1953) 212–213, https://doi.org/10.1103/PhysRev.92.212.2.
[3] E.P. Saliba, E.L. Sesti, F.J. Scott, B.J. Albert, E.J. Choi, N. Alaniva, C. Gao, A.B. Barnes, Electron decoupling with dynamic nuclear polarization in rotating solids, J. Am. Chem. Soc. 139 (2017) 6310–6313, https://doi.org/10.1021/jacs.7b02714.
[4] B.J. Albert, C. Gao, E.L. Sesti, E.P. Saliba, N. Alaniva, F.J. Scott, S.T. Sigurdsson, A. B. Barnes, Dynamic nuclear polarization nuclear magnetic resonance in human cells using fluorescent polarizing agents, Biochemistry 57 (2018) 4741–4746, https://doi.org/10.1021/acs.biochem.8b00257.
[5] A. Zagdoun, G. Casano, O. Ouari, M. Schwarzwälder, A.J. Rossini, F. Aussenac, M. Yulikov, G. Jeschke, C. Copéret, A. Lesage, P. Tordo, L. Emsley, Large molecular weight nitroxide biradicals providing efficient dynamic nuclear polarization at temperatures up to 200 K, J. Am. Chem. Soc. 135 (2013) 12790–12797, https://doi.org/10.1021/ja405813t.
[6] L.R. Becerra, G.J. Gerfen, R.J. Temkin, D.J. Singel, R.G. Griffin, Dynamic nuclear polarization with a cyclotron resonance maser at 5 T, Phys. Rev. Lett. 71 (1993) 3561–3564, https://doi.org/10.1103/PhysRevLett.71.3561.
[7] T. Kobayashi, F.A. Perras, I.I. Slowing, A.D. Sadow, M. Pruski, Dynamic nuclear polarization solid-state NMR in heterogeneous catalysis research, ACS Catal. 5 (2015) 7055–7062, https://doi.org/10.1021/acscatal.5b02039.
[8] D.J. Kubicki, A.J. Rossini, A. Purea, A. Zagdoun, O. Ouari, P. Tordo, F. Engelke, A. Lesage, L. Emsley, Amplifying dynamic nuclear polarization of frozen solutions by incorporating dielectric particles, J. Am. Chem. Soc. 136 (2014) 15711–15718, https://doi.org/10.1021/ja5088453.
[9] T.V. Can, M.A. Caporini, F. Mentink-Vigier, B. Corzilius, J.J. Walish, M. Rosay, W. E. Maas, M. Baldus, S. Vega, T.M. Swager, R.G. Griffin, Overhauser effects in insulating solids, J. Chem. Phys. 141 (2014) 064202, https://doi.org/10.1063/1.4891866.
[10] A.N. Smith, M.A. Caporini, G.E. Fanucci, J.R. Long, A method for dynamic nuclear polarization enhancement of membrane proteins, Angew. Chem. Int. Ed. 54 (2015) 1542–1546, https://doi.org/10.1002/anie.201410249.
[11] B.J. Wylie, B.G. Dzikovski, S. Pawsey, M. Caporini, M. Rosay, J.H. Freed, A.E. McDermott, Dynamic nuclear polarization of membrane proteins: covalently bound spin-labels at protein-protein interfaces, J. Biomol. NMR 61 (2015) 361–367, https://doi.org/10.1007/s10858-015-9919-6.
[12] A.B. Barnes, E.A. Nanni, J. Herzfeld, R.G. Griffin, R.J. Temkin, A 250 GHz gyrotron with a 3 GHz tuning bandwidth for dynamic nuclear polarization, J. Magn. Reson. 221 (2012) 147–153, https://doi.org/10.1016/j.jmr.2012.03.014.
[13] F. Mentink-Vigier, G. Mathies, Y. Liu, A.-L. Barra, M.A. Caporini, D. Lee, S. Hediger, R.G. Griffin, G. De Paëpe, Efficient cross-effect dynamic nuclear polarization without depolarization in high-resolution MAS NMR, Chem. Sci. (2017), https://doi.org/10.1039/C7SC02199B.
[14] E.P. Saliba, E.L. Sesti, N. Alaniva, A.B. Barnes, Pulsed electron decoupling and strategies for time domain dynamic nuclear polarization with magic angle spinning, J. Phys. Chem. Lett. 9 (2018) 5539–5547, https://doi.org/10.1021/acs.jpclett.8b01695.
[15] T.V. Can, R.T. Weber, J.J. Walish, T.M. Swager, R.G. Griffin, Frequency-swept integrated solid effect, Angew. Chem. Int. Ed. 56 (2017) 6744–6748, https://doi.org/10.1002/anie.201700032.
[16] K.R. Thurber, R. Tycko, Theory for cross effect dynamic nuclear polarization under magic-angle spinning in solid state nuclear magnetic resonance: the importance of level crossings, J. Chem. Phys. 137 (2012), https://doi.org/10.1063/1.4747449.
[17] X. Wang, B.G. Caulkins, G. Riviere, L.J. Mueller, F. Mentink-Vigier, J.R. Long, Direct dynamic nuclear polarization of 15 N and trityl radical and magic angle spinning C spins at 14. 1 T using a trityl radical and magic angle spinning, 100 (2019) 85–91. doi: 10.1016/j.ssnmr.2019.03.009.
[18] A.S. Lilly Thankamony, J.J. Wittmann, M. Kaushik, B. Corzilius, Dynamic nuclear polarization for sensitivity enhancement in modern solid-state NMR, Prog. Nucl. Magn. Reson. Spectrosc. 102–103 (2017) 120–195, https://doi.org/10.1016/j.pnmrs.2017.06.002.
[19] M. Lelli, S.R. Chaudhari, D. Gajan, G. Casano, A.J. Rossini, O. Ouari, P. Tordo, A. Lesage, L. Emsley, Solid-state dynamic nuclear polarization at 9.4 and 18.8 T from 100 K to room temperature, J. Am. Chem. Soc. 137 (2015) 14558–14561, https://doi.org/10.1021/jacs.5b08423.
[20] M. Afeworki, R.A. McKay, J. Schaefer, Selective observation of the interface of heterogeneous polycarbonate/polystyrene blends by dynamic nuclear polarization carbon-13 NMR spectroscopy, Macromolecules 25 (1992) 4084–4091, https://doi.org/10.1021/ma00042a006.
[21] A.B. Barnes, B. Corzilius, M.L. Mak-Jurkauskas, L.B. Andreas, V.S. Bajaj, Y. Matsuki, M.L. Belenky, J. Lugtenburg, J.R. Sirigiri, R.J. Temkin, J. Herzfeld, R.G. Griffin, Resolution and polarization distribution in cryogenic DNP/MAS experiments, PCCP 12 (2010) 5741–5751, https://doi.org/10.1039/c002146f.
[22] E.L. Sesti, E.P. Saliba, N. Alaniva, A.B. Barnes, Electron decoupling with cross polarization and dynamic nuclear polrization below 6 K, J. Magn. Reson. 295 (2018) 1–5, https://doi.org/10.1016/J.JMR.2018.07.016.
[23] A.B. Siemer, K.Y. Huang, A.E. McDermott, Protein Linewidth and Solvent Dynamics in Frozen Solution NMR, PLoS ONE 7 (2012), https://doi.org/10.1371/journal.pone.0047242.
[24] B. Corzilius, Theory of solid effect and cross effect dynamic nuclear polarization with half-integer high-spin metal polarizing agents in rotating solids, PCCP 18 (2016) 27190–27204, https://doi.org/10.1039/c6cp04621e.
[25] T. Maly, G.T. Debelouchina, V.S. Bajaj, K.-N. Hu, C.-G. Joo, M.L. Mak-Jurkauskas, J.R. Sirigiri, P.C.A. van der Wel, J. Herzfeld, R.J. Temkin, R.G. Griffin, Dynamic nuclear polarization at high magnetic fields, J. Chem. Phys. 128 (2008) 052211, https://doi.org/10.1063/1.2833582.
[26] A. Henstra, P. Dirksen, W.T. Wenckebach, Enhanced dynamic nuclear polarization by the integrated solid effect, Phys. Lett. A 134 (1988) 134–136, https://doi.org/10.1016/0375-9601(88)90950-4.
[27] T.V. Can, J.J. Walish, T.M. Swager, R.G. Griffin, Time domain DNP with the NOVEL sequence, J. Chem. Phys. 143 (2015) 1–8, https://doi.org/10.1063/1.4927087.
[28] A. Henstra, P. Dirksen, J. Schmidt, W.T. Wenckebach, Nuclear Spin Orientation via Electron Spin Locking (NOVEL), J. Magn. Reson. 77 (1988) 389–393, https://doi.org/10.1016/0022-2364(88)90190-4.
[29] K.O. Tan, C. Yang, R.T. Weber, G. Mathies, R.G. Griffin, Time-optimized pulsed dynamic nuclear polarization, Sci. Adv. 5 (2019) 1–8, https://doi.org/10.1126/sciadv.aav6909.
[30] I. Kaminker, S. Han, Amplification of dynamic nuclear polarization at 200 GHz by arbitrary pulse shaping of the electron spin saturation profile, J. Phys. Chem. Lett. 9 (2018) 3110–3115, https://doi.org/10.1021/acs.jpclett.8b01413.
[31] A. Bornet, J. Milani, B. Vuichoud, A.J. Perez Linde, G. Bodenhausen, S. Jannin, Microwave frequency modulation to enhance dissolution dynamic nuclear polarization dedicated to martial Rey, as a token of appreciation, Chem. Phys. Lett. 602 (2014) 63–67, https://doi.org/10.1016/j.cplett.2014.04.013.
[32] C. Gao, N. Alaniva, E.P. Saliba, E.L. Sesti, P.T. Judge, F.J. Scott, T. Halbritter, S.T. Sigurdsson, A.B. Barnes, Frequency-chirped dynamic nuclear polarization with magic angle spinning using a frequency-agile Gyrotron, J. Magn. Reson. 308 (2019) 106586, https://doi.org/10.1016/j.jmr.2019.106586.
[33] A. Equbal, K. Tagami, S. Han, Pulse shaped dynamic nuclear polarization under magic angle spinning, J. Phys. Chem. Lett. (2019), https://doi.org/10.26434/chemrxiv.9788471.v1.
[34] V.S. Bajaj, M.L. Mak-Jurkauskas, M. Belenky, J. Herzfeld, R.G. Griffin, Functional and shunt states of bacteriorhodopsin resolved by 250 GHz dynamic nuclear polarization-enhanced solid-state NMR, Proc. Natl. Acad. Sci. USA 106 (2009) 9244–9249, https://doi.org/10.1073/pnas.0900908106.
[35] R.W. Martin, R.C. Jachmann, D. Sakellariou, U.G. Nielsen, A. Pines, High-resolution nuclear magnetic resonance spectroscopy of biological tissues using projected magic angle spinning, Magn. Reson. Med. 54 (2005) 253–257, https://doi.org/10.1002/mrm.20585.
[36] W. Tang, A. Bhatt, A.N. Smith, P.J. Crowley, L.J. Brady, J.R. Long, Specific binding of a naturally occurring amyloidogenic fragment of Streptococcus mutans adhesin P1 to intact P1 on the cell surface characterized by solid state NMR spectroscopy, J. Biomol. NMR 64 (2016) 153–164, https://doi.org/10.1007/s10858-016-0017-1.
[37] S.H. Werby, L. Cegelski, Spectral comparisons of mammalian cells and intact organelles by solid-state NMR, J. Struct. Biol. 206 (2019) 49–54, https://doi.org/10.1016/j.jsb.2018.05.007.
[38] R. Gupta, H. Zhang, M. Lu, G. Hou, M. Caporini, M. Rosay, W. Maas, J. Struppe, J. Ahn, I.J.L. Byeon, H. Oschkinat, K. Jaudzems, E. Barbet-Massin, L. Emsley, G. Pintacuda, A. Lesage, A.M. Gronenborn, T. Polenova, Dynamic nuclear polarization magic-angle spinning nuclear magnetic resonance combined with molecular dynamics simulations permits detection of order and disorder in viral assemblies, J. Phys. Chem. B 123 (2019) 5048–5058, https://doi.org/10.1021/acs.jpcb.9b02293.
[39] F.J. Scott, E.P. Saliba, B.J. Albert, N. Alaniva, E.L. Sesti, C. Gao, N.C. Golota, E.J. Choi, A.P. Jagtap, J.J. Wittmann, M. Eckardt, W. Harneit, B. Corzilius, S.Th.

Sigurdsson, A.B. Barnes, Frequency-agile gyrotron for electron decoupling and pulsed dynamic nuclear polarization, J. Magn. Reson. 289 (2018) 45–54, https://doi.org/10.1016/j.jmr.2018.02.010.

[40] P.T. Judge, E.L. Sesti, E.P. Saliba, N. Alaniva, T. Halbritter, S.T. Sigurdsson, A.B. Barnes, Sensitivity analysis of magic angle spinning dynamic nuclear polarization below 6 K, J. Magn. Reson. 305 (2019) 51–57, https://doi.org/10.1016/j.jmr.2019.05.011.

[41] F.J. Scott, N. Alaniva, N.C. Golota, E.L. Sesti, E.P. Saliba, L.E. Price, B.J. Albert, P. Chen, R.D. O'Connor, A.B. Barnes, A versatile custom cryostat for dynamic nuclear polarization supports multiple cryogenic magic angle spinning transmission line probes, J. Magn. Reson. 297 (2018) 23–32, https://doi.org/10.1016/J.JMR.2018.10.002.

[42] C.M. Rienstra, A.E. Bennett, R.G. Griffin, K.V. Lakshmi, M. Auger, Heteronuclear decoupling in rotating solids, J. Chem. Phys. 103 (2002) 6951–6958, https://doi.org/10.1063/1.470372.

[43] D.E.M. Hoff, B.J. Albert, E.P. Saliba, F.J. Scott, E.J. Choi, M. Mardini, A.B. Barnes, Frequency swept microwaves for hyperfine decoupling and time domain dynamic nuclear polarization, Solid State Nucl. Magn. Reson. 72 (2015) 79–89, https://doi.org/10.1016/j.ssnmr.2015.10.001.

[44] D. Massiot, F. Fayon, M. Capron, I. King, S. Le Calvé, B. Alonso, J.O. Durand, B. Bujoli, Z. Gan, G. Hoatson, Modelling one- and two-dimensional solid-state NMR spectra, Magn. Reson. Chem. 40 (2002) 70–76, https://doi.org/10.1002/mrc.984.

[45] G. Mathies, M.A. Caporini, V.K. Michaelis, Y. Liu, K.N. Hu, D. Mance, J.L. Zweier, M. Rosay, M. Baldus, R.G. Griffin, Efficient dynamic nuclear polarization at 800 MHz/527 GHz with trityl-nitroxide biradicals, Angew. Chem. Int. Ed. 54 (2015) 11770–11774, https://doi.org/10.1002/anie.201504292.

[46] F. Mentink-Vigier, S. Paul, D. Lee, A. Feintuch, S. Hediger, S. Vega, G. De Paëpe, Nuclear depolarization and absolute sensitivity in magic-angle spinning cross effect dynamic nuclear polarization, PCCP 17 (2015) 21824–21836, https://doi.org/10.1039/C5CP03457D.

[47] T.A. Siaw, M. Fehr, A. Lund, A. Latimer, S.A. Walker, D.T. Edwards, S.I. Han, Effect of electron spin dynamics on solid-state dynamic nuclear polarization performance, PCCP 16 (2014) 18694–18706, https://doi.org/10.1039/c4cp02013h.